CrossMark

Precipitation of Spherical Vaterite Particles via Carbonation Route in the Bubble Column and the Gas-Lift Reactor

DONATA KONOPACKA-ŁYSKAWA [iD],[1,3] BARBARA KOŚCIELSKA,[2] and
MARCIN ŁAPIŃSKI[2]

1.—Department of Chemical and Process Engineering, Faculty of Chemistry, Gdańsk University
of Technology, Narutowicza 11/12, 80-233 Gdańsk, Poland. 2.—Department of Solid State Physics,
Faculty of Applied Physics and Mathematics, Gdańsk University of Technology, Narutowicza 11/
12, 80-233 Gdańsk, Poland. 3.—e-mail: donata.konopacka-lyskawa@pg.edu.pl

Spherical vaterite particles were produced by carbonation of calcium chloride
solution with addition of ammonia to facilitate CO_2 absorption. Synthesis of
calcium carbonate was carried out in a bubble column or gas-lift reactor. The
course of the reaction was monitored by pH measurements. Precipitated solids
were analyzed by Fourier-transformed infrared spectroscopy, x-ray powder
diffraction and scanning electron microscopy, and the particle size distribution
was determined by a laser diffraction method. Synthesized calcium carbonate
products were mainly vaterite. The calcium chloride concentration and carbon
dioxide volume fraction in a gas phase had the main impact on the size of the
produced particles in both reactors. A slight decrease in the mean particle size
was observed for the highest mixing intensity. Both tested reactors can be
applied to produce vaterite particles, although formation of homogeneous non-
agglomerated spherical particles in a gas-lift reactor required careful selection
of the process parameters.

INTRODUCTION

Calcium carbonate is a compound that occurs extensively in nature, and it is produced on a large scale by the chemical industry. It can crystallize as three anhydrous polymorphs: calcite, aragonite and vaterite. The least stable polymorph is vaterite, which relatively easily transforms into more stable forms, i.e., calcite (the most stable polymorph), at temperatures $< 40°C$ or aragonite at higher temperatures.[1,2] Vaterite has a hexagonal crystal system, and all vaterite structures belong to the order–disorder (OD) family.[3] This means that the occurrence of multiple polytypes on the micro- to macroscopic scale and considerable stacking disorder are both to be expected.

Vaterite has a broad range of applications both in personal care products and for biomedical purposes because of it nontoxicity, good biocompatibility and affinity, low cost and ease of large-scale production. Calcium carbonate in a vaterite form is used as an abrasive, absorbent, anticaking agent, buffer, filler, colorant and emulsion stabilizer.[4] Also, spherical vaterite particles have been proposed as a delivery carrier for drugs and bioactive proteins.[5–7]

The controlled precipitation of calcium carbonate to produce a specific polymorph was described in many research papers. Factors influencing the formation of a given crystalline form were divided into primary and secondary parameters by Kitamura.[8] Supersaturation, temperature, stirring rate, mixing rate of reactant solutions and antisolvents as well as seed crystals are the primary factors, while the type of solvent, additives, interface, pH and host–guest composition are secondary factors. It has been found that high supersaturation,[8,9] low temperature[1,4] and the addition of polyols[4,10] or ammonia and some amines[11,12] into the reactive mixtures as well as using ethanol as a solvent for precipitation[13,14] favor the precipitation of calcium carbonate in the vaterite form. The role of pH in vaterite synthesis is not clear, because some researchers found that pH > 9 favors vaterite precipitation,[2,15] others that vaterite is formed in solutions of pH < 8[16] or of pH in the range between 7.5 and 9.5.[12] The influence of mixing intensity on vaterite precipitation has not been reported, but the size of the final particles usually decreases with an increase of mixing rate when calcite[17–20] or aragonite[21] crystals are formed.

$CaCO_3$ synthesis can be carried out in several ways: (1) by mixing the solution of soluble calcium salt with the solution containing soluble carbonate salts; (2) by carbonation of calcium hydroxide slurry with carbon dioxide[22] or carbonation of soluble calcium salt solution containing CO_2 absorption promoters such as ammonia and amines;[11,23,24] (3) CO_2 diffusion method;[25,26] (4) precipitation of calcium carbonate by carbon dioxide formed in situ during hydrolysis of CO_2 precursors such as urea or ammonium carbamate[9,27] and during photodegradation of some organic compounds.[28] Almost all of the above methods can be applied for pure vaterite formation by adjusting the process parameters discussed earlier, but precipitation via carbonation of the calcium hydroxide slurry probably requires the use of a different solvent than water, e.g., ethanol–water solution (at an ethanol concentration > 60%) allowed to obtain a mixture of vaterite, aragonite and calcite as the final product.[14]

In this work, the synthesis of vaterite was carried out via carbonation of solution containing calcium chloride and ammonia. Precipitation in gas–liquid–solid systems mostly requires the generation of a gas–liquid contact to enable a good mass transfer from a gas to a liquid phase and enough circulation to avoid settling of the produced calcium carbonate particles. These conditions can be controlled by selecting the appropriate reactor design to conduct the precipitation. Reactors for gas–liquid precipitation can be operated by gas bubble dispersion into liquid or droplet dispersion in gas phase.[17] In laboratory practice, reactors used to carry out calcium carbonate precipitation with gaseous carbon dioxide are usually stirrer tanks equipped with a gas distributor[14,29,30] or bubble columns.[12,31] To model the precipitation process, agitated vessels with a flat gas–liquid surface were used.[32,33] Also, reactors with special constructions such as a gas-lift reactor,[17,19,34] multistage column crystallizer,[35] spinning disc reactor,[36] Couette–Taylor reactor,[37] rotating disc precipitation reactor,[38] membrane dispersion minireactor[18] and high-gravity rotating packed bed reactor[39,40] have been applied.

No studies have shown the comparison of the precipitation process carried out in a bubble column and in a bubble column with a draft tube, which is a type of a gas-lift reactor with internal circulation. Therefore, the aim of this work is to compare the vaterite production in these two types of reactors. The main difference between gas-lift reactors and bubble columns is the type of fluid flow.[41] Usually, the gas is supplied in the bottom of the bubble column and the ascending gas bubbles produce random mixing. However, the presence of a draft tube in a gas-lift reactor results in the separation of the riser and downcomer zones. The gas is supplied in the bottom of the riser and flows up to the zone at the top of the column, called the gas separator, where some gas fraction is separated while the residual gas fraction is entrapped by the descending liquid and taken into the downcomer. As a result, special conditions of mixing and mass exchange in the gas-lift reactor are generated.

EXPERIMENTAL

Reagents

Calcium chloride, anhydrous (Eurochem BGD), and ammonium hydroxide solution 25% in water (CHEMPUR) were of analytical reagent grade and were used in this study without further purification. Water purified by reverse osmosis (RO) was used to prepare all solutions. Carbon dioxide was purchased from Oxygen s.c.

Preparation

Calcium carbonate was precipitated in a bubble column with or without a coaxial column placed inside a reactor as a draft tube. The outer column diameter was D_o/D_i = 80/72 mm and its height 690 mm. The draft-tube diameter was d_o/d_i = 40/36 mm and the height 450 mm, and it was placed 35 mm above the bottom of the reactor. The gas distributor was a part of the bottom of the reactor and was made with a 20-mm-diameter Teflon circular plate with 13 uniformly arranged holes of 0.5 mm diameter. The pH probe was located in the gas separator zone. The reading of the volumetric gas flow rate was corrected to the atmospheric conditions at the top of the reactor by pressure and temperature measured under the gas distributor. The corrected volume flow rate of the gas and the cross- sectional area of the outer column or inner column were used to calculate the superficial gas velocity in a bubble column or in a bubble column with a draft tube, respectively. The experiments were carried out in a semi-batch manner. Solutions used in experiments contained from 0.2 M to 0.6 M calcium chloride. The ammonia used as a CO_2 promoter was added to obtain the ratio of $NH_3/CaCl_2$ equal to 1.5 in all experiments. The gas flow rate was from 60 dm^3/h to 180 dm^3/h. A volume fraction of carbon dioxide in a gas stream supplied to the reactor was 0.15, 0.575, and 1. The initial supersaturation ratios were calculated according the relationship S1 in the supplementary materials. A summary of the process conditions is provided in Table I. The concentration of calcium ions in collected samples was determined after $CaCO_3$ particle filtration by the titration method with disodium salt of ethylene diaminetetraacetic acid (EDTA). The produced $CaCO_3$ precipitates were filtered, washed with ethanol and dried at 100°C for 12 h.

Characterization of $CaCO_3$ particles

The size of calcium carbonate particles was determined by a laser diffraction method (LS13320, Beckman Coulter). Precipitated particles were observed by a microscope (Delta Optical ME1000 equipped with a digital camera and a

Table I. Experimental conditions in vaterite precipitation

Symbol	C_{CaCl_2}, mol/dm^3	V_G, dm^3/h	x_V, −	S_i
Gas-lift reactor				
A1	0.2	60	1	220
A3	0.2	120	1	220
A5	0.2	180	1	220
A6	0.4	120	1	486
A7	0.6	120	1	1078
A8	0.2	120	0.15	85
A9	0.2	120	0.575	167
Bubble column				
B1	0.2	60	1	220
B3	0.2	120	1	220
B5	0.2	180	1	220
B6	0.4	120	1	486
B7	0.6	120	1	1078
B8	0.2	120	0.15	85
B9	0.2	120	0.575	167

C_{CaCl_2}, calcium chloride concentration; V_G, volume flow rate of gas phase; x_V, volume fraction of CO_2 in gas phase; S_i, initial saturation ratio.

computer; effective magnification used ×3200). To determine the crystalline structure of samples and to characterize the polymorph composition of calcium carbonate, the conventional x-ray powder diffraction (XRD) technique (Philips X'Pert diffractometer system) with Co-K$_\alpha$ radiation was used. The XRD spectra were collected at a scan rate 0.2° and 2θ range 20°–60° at room temperature. Taking into account the precision of the measuring system, the sensibility of the proposed method was about 2%. The types of chemical bonds in the structural units present in the samples were identified using Fourier transform infrared spectroscopy (FTIR). Measurements were carried out on a Tensor 27 (Bruker) at room temperature. The FTIR method is highly sensitive and allows detection in a test sample of even small quantities of the substance of < 0.1%. The FT-IR spectra were obtained between 4000 cm^{-1} and 400 cm^{-1} using an average of 264 scannings at 2 cm^{-1} resolution. Both the XRD and FT-IR measurements were repeated for several samples obtained under the same conditions. For the particle characterization, an FEI Quanta FEG 250 scanning electron microscope (SEM) with an Everhart–Thornley (ET) secondary electron detector was used.

RESULTS AND DISCUSSION

Calcium carbonate precipitation was carried out under pH control. The end of precipitation was when the pH value decreased to 7. Courses of pH versus time for various carbon dioxide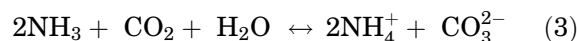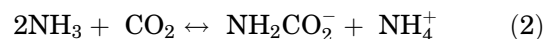 flows in a gas-lift reactor and in a bubble column are presented in Fig. 1. Changes of pH over time during $CaCO_3$ precipitation in both reactors to compare the influence of the calcium chloride concentration and of the CO_2 volume fraction in a gas phase are shown in supplementary materials Fig. S-1 and Fig. S-2.

The consumption of calcium ions in the reaction was calculated on the basis of the determination of the Ca^{2+} concentration in the initial solutions and filtrates obtained after $CaCO_3$ particle separation from reaction mixtures, and the results are shown in Table II. The efficiency of the calcium carbonate precipitation was comparable in all experiments and was around 70%, although slightly better results were obtained when the process was carried out in the gas-lift reactor.
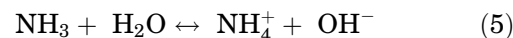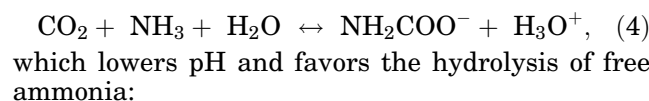
The decrease of pH values during the carbonation of calcium chloride solution in the presence of ammonia is a result of several reactions that can be written in total as[12]:

$$Ca^{2+}(aq) + 2NH_4OH(aq) + CO_2(g) \rightarrow CaCO_3(s) + 2NH_4^+(aq) + H_2O(aq) \quad (1)$$
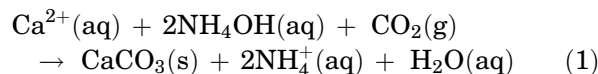
The detailed research on CO_2 absorption into ammonia solution[42] has shown that the excess of ammonia favors carbamate and carbonate ion formation, and in this case the overall reactions can be written as:

$$2NH_3 + CO_2 \leftrightarrow NH_2CO_2^- + NH_4^+ \quad (2)$$

$$2NH_3 + CO_2 + H_2O \leftrightarrow 2NH_4^+ + CO_3^{2-} \quad (3)$$

Carbamate formation is accompanied by H_3O^+ generation:

$$CO_2 + NH_3 + H_2O \leftrightarrow NH_2COO^- + H_3O^+, \quad (4)$$

which lowers pH and favors the hydrolysis of free ammonia:

$$NH_3 + H_2O \leftrightarrow NH_4^+ + OH^- \quad (5)$$

Precipitation of calcium carbonate occurs when the concentrations of Ca^{2+} and CO_3^{2-} exceed the value of the solubility product. The visual observation of reactive mixtures is one way to estimate an experimental induction period, which is defined as a time that elapses between the creation of supersaturation and the first observable change of the precipitating system.[43] The appearance of the first crystals in the reactive mixtures was monitored. A comparison of the observed turbidity time and time of completion of the carbonation carried out in both reactors is collected in Table II and shown in Fig. S-3. A slight increase in the time of the appearance of first calcium carbonate particles was observed when the reaction was carried out in the gas-lift reactor, although the differences in the induction time were not significant for the same precipitation conditions in both reactors. However, the time of the end of precipitation, which was established when the pH value of solutions was 7, was higher in the gas-lift
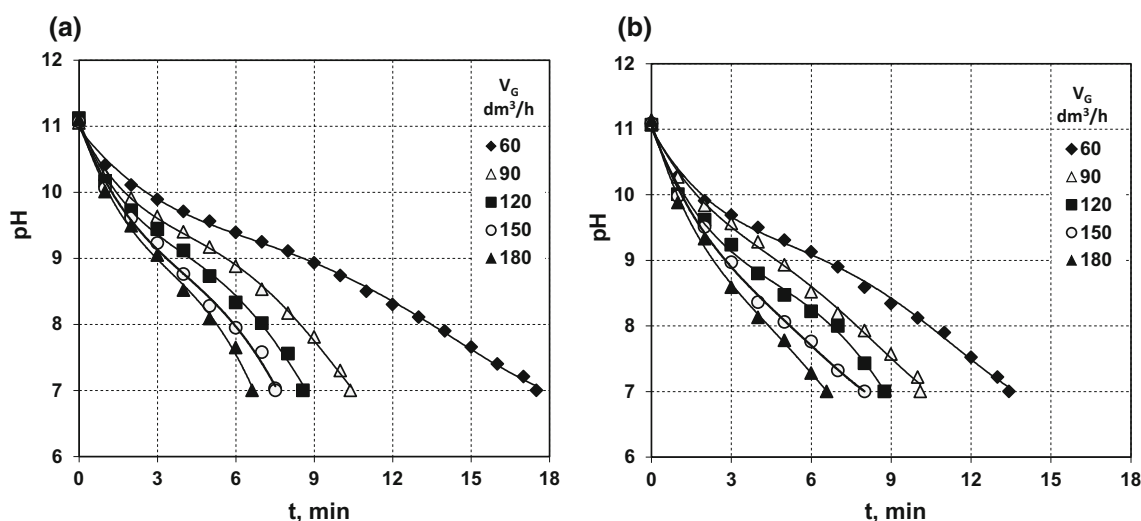
Fig. 1. pH values of reactive mixture versus time depending on the volume flow rate of carbon dioxide (V_G) in a gas-lift reactor (a) and in a bubble column (b).

Table II. Appearance of turbidity (initial time), the end time of the reaction, calcium ion consumption, polymorphic composition, crystallite size and particle size of synthesized particles

Symbol	τ_t, s	τ_r, s	ΔC_{CaCl_2}, %	% V	$d_{c,V}$, nm	d_{p50}, μm	r_{cr}, nm	d_{cal}, μm
A1	260	1050	69	97.0	50	11.1	0.3	11.3
A3	123	514	68	95.8	40	11.4	0.3	8.1
A5	130	397	70	97.8	40	10.1	0.3	7.1
A6	205	848	71	99.6	40	9.0	0.3	14.0
A7	222	1110	71	94.5	34	7.4	0.3	13.3
A8	580	3242	73	97.5	46	21.8	0.4	12.6
A9	309	1174	66	99.9	46	10.5	0.4	10.6
B1	230	806	69	86.4	44	11.0	0.3	10.1
B3	165	525	65	89.4	44	13.0	0.3	8.2
B5	128	395	68	93.3	44	10.1	0.3	7.2
B6	175	747	71	99.9	32	10.6	0.3	13.0
B7	250	950	68	91.0	44	8.6	0.3	12.1
B8	570	2604	66	97.8	40	14.8	0.4	11.4
B9	230	800	66	99.9	33	9.2	0.4	8.8

τ_t intial time; τ_r, reaction time; ΔC_{CaCl_2}, calcium ion consumption; % V, % of vaterite in the product; $d_{c,V}$, crystallite size of vaterite; d_{p50}, mean particle size; r_{cr}, critical radius of nuclei; d_{cal}, estimated size of the particle.

reactor. More significant differences in reaction time were observed when the carbon dioxide flow was lower (i.e., 60 dm³/h and 90 dm³/h), the concentration of calcium chloride and ammonia was higher (0.6 M and 0.9 M, respectively), and the volume fraction of carbon dioxide in the gas stream was lower (0.15). The explanation of the variation in reaction time can be a comparison of the hydrodynamics and mass transfer in airlift and bubble column reactors. Baten and Krishna[44] applied computational fluid dynamics (CFD) techniques to discuss this problem and showed that the liquid circulation is much stronger in airlifts than in bubble columns. The gas hold-up is lower in airlifts compared with bubble columns at the same superficial gas velocity, and the volumetric mass transfer coefficient is lower in airlifts. Also, the mixing times were shorter in a bubble column compared with the airlift reactor for the same volume flow rate of the gas phase.[45] Thus, an increase in a reaction time between the reagent in a solution and carbon dioxide supplied as a gaseous reactant in a gas-lift reactor can be elucidated by the slower mass transfer from gas to the liquid phase compared with a bubble column. The differences in the observed reaction time are greater when the concentrations of reactants in both a liquid and gas phase are higher.

Precipitation of Spherical Vaterite Particles via Carbonation Route in the Bubble Column and
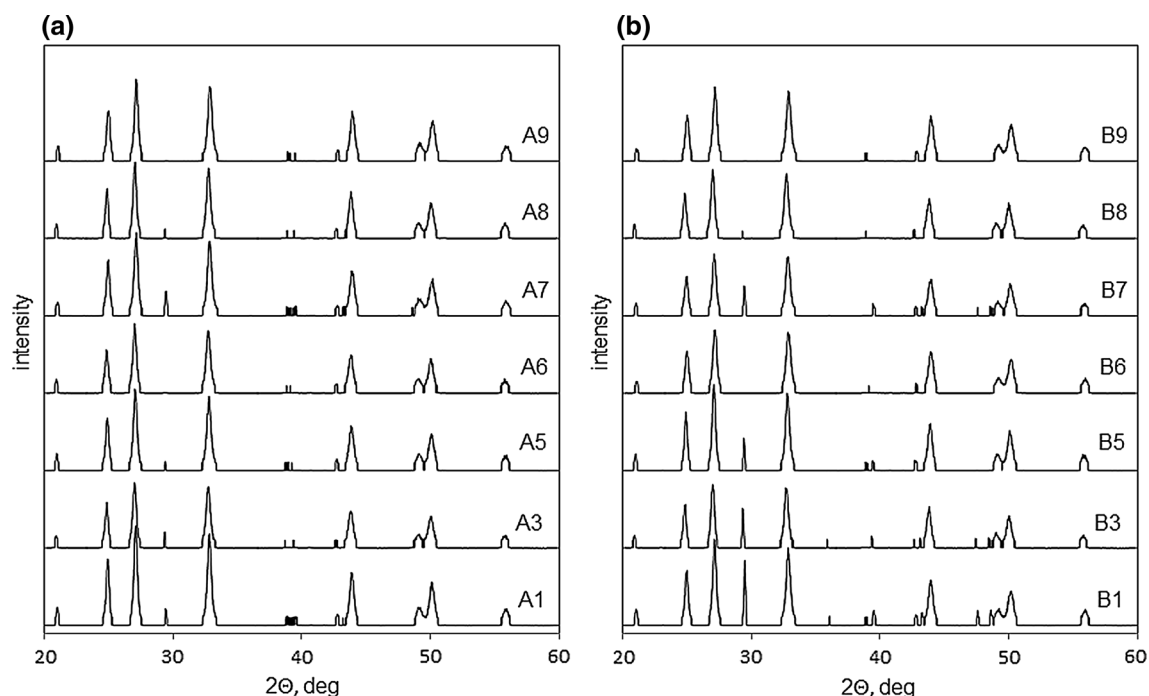the Gas-Lift Reactor

Fig. 2. XRD pattern of calcium carbonate particles produced in a gas-lift reactor (a) and in a bubble column (b); description of sample symbols are shown in Table I.

Precipitated calcium carbonate particles were analyzed by FTIR and XRD. The results of XRD measurements are presented in Fig. 2, and FTIR spectra are shown in the supplementary materials in Fig. S-4. Characteristic peaks for vaterite are seen in the XRD results and FTIR spectra performed for all calcium carbonate samples. A small amount of calcite is also detected in the analyzed products. The share of vaterite in vaterite-calcite precipitates was calculated based on the equation[46]:

$$X_V = \frac{7.691(I_V^{110})}{I_C^{104} + 7.691(I_V^{110})} \tag{6}$$

where X_V is a fraction of vaterite in the calcite-vaterite mixture; I_V^{110} is the intensity of the reflection peak at (110) for vaterite and I_C^{104} at (104) for calcite. The concentrations of vaterite in the calcium carbonate samples are shown in Table II. Usually, for the same reaction conditions, calcium carbonate particles with a higher concentration of vaterite were obtained in the gas-lift reactor.

Precipitation of calcium carbonate in the presence of ammonia promotes the formation of vaterite.[11,12,23] High pH of the reactive mixture caused by an addition of ammonia generates a high supersaturation and nucleation rate that favors precipitation of a less stable polymorph, i.e., vaterite.[8] Also, carbamates created during carbon dioxide absorption in ammonia (Eq. 4) may stabilize vaterite particles.[9,11] The following steps are distinguished during calcium carbonate precipitation: formation of amorphous calcium carbonate, then its rapid dehydration to vaterite particles and

slower vaterite transformation to more stable calcite by the dissolution–recrystallization process.[47] Both consumption of calcium ions in the reaction and the decrease in pH value at the end of precipitation result in the reduction of supersaturation and decreasing of the rate of vaterite formation. According to Udrea et al.[12] the long carbonation time and low pH (about 6.5) favor transformation of vaterite into calcite by the dissolution–recrystallization mechanism, while Han et al.[15] found that vaterite can be transformed relatively quickly at high pH. However, in our experiments, a lower vaterite concentration was in calcium carbonate samples precipitated in the bubble column with pure carbon dioxide (i.e., in samples B1, B3, B5, B7) compared with calcium carbonate particles produced in the gas-lift reactor. During carbonation, transformation of vaterite into calcite takes place simultaneously with continuous CO_2 absorption, gas–liquid reaction and precipitation. Mass transfer from gas to liquid phase occurs faster in a bubble column than in a gas-lift reactor;[44] therefore, a higher supersaturation generated by CO_2 absorption can be achieved in a shorter time, formation of vaterite particles is more rapid, and its transformation may start earlier.

The morphology of the obtained vaterite particles was determined on the basis of the SEM images presented in Fig. 3 and in supplementary materials in Fig. S-5 and Fig. S-6. Spherical vaterite particles were the main product in all experiments. However, careful analysis of images shows that the synthesized particles are framboidal aggregates composed
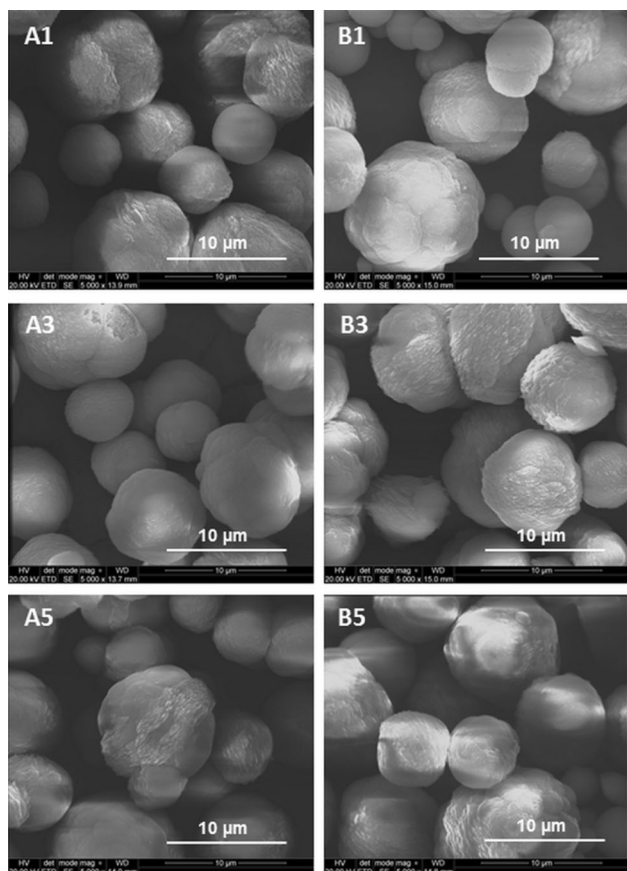
Fig. 3. SEM images of calcium carbonate particles precipitated in a gas-lift reactor (a) and a bubble column (b) for different pure CO_2 flow rates; description of sample symbols are shown in Table I.

Fig. 4. Particle size distribution of calcium carbonate particles produced in a gas-lift reactor (a) and bubble column (b) for various $CaCl_2$ initial concentrations; CO_2 flow rate, 120 dm^3/h.

of smaller units. The sizes of crystallites can be estimated from XRD analysis using the Scherrer formula, and the obtained values are shown in Table II. The crystallite-forming particles produced in both reactors are comparable in size. The critical sizes of nuclei estimated according the classical theory of nucleation (Eq. S2 in supplementary materials) included in Table II are also similar for all tested precipitation conditions. Nevertheless, vaterite particles precipitated in the bubble column more often form shapes composed of smaller sphere sections (e.g., sample B1, B5, B6, B8), which may indicate that a higher rate of reaction and intense mixing causes increased deformation of the spherical growth characteristic for vaterite particles. Similar vaterite morphology is observed when the highest gas flow rate is used in the gas-lift reactor (sample A5).

Particle size distributions (PSDs) of produced particles determined by a laser diffraction analysis are shown in Fig. 4 as well as supplementary materials in Fig. S-7 and Fig. S-8, and the mean particle sizes d_{p50} are shown in Table II. For comparison, the size of particles estimated using the e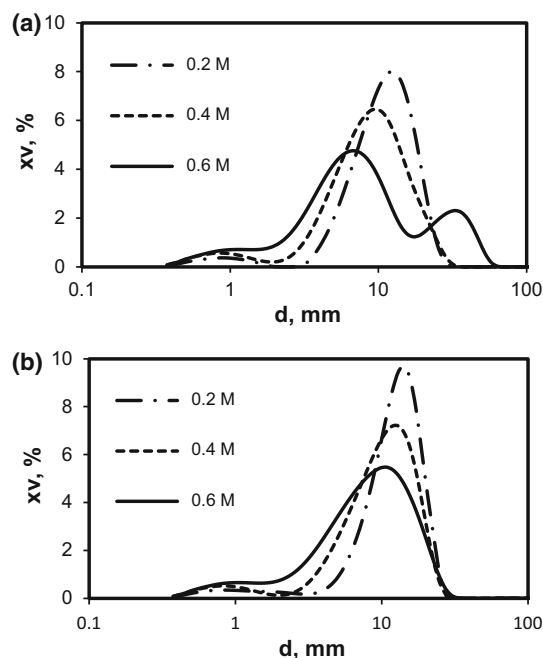quation for the diffusion-controlled linear growth rate is also shown in Table II. Details and data for calculation are presented in the supplementary materials.

The value of d_{p50} is the median of the particle population. D_{p50} values of particles obtained under similar reaction conditions in both reactors are comparable, but when a gas stream with the lowest CO_2 content ($x_V = 0.15$) was used in the reaction, the mean size of particles synthesized in the gas-lift reactor is significantly larger. Particle size distributions for all vaterite particles have multimodal courses with a small peak around 1 μm. In addition, a peak around 13 μm diameter has been registered for particles obtained in the gas-lift reactor when the gas flow rate of pure CO_2 was 60 dm^3/h or 90 dm^3/h and the initial $CaCl_2$ concentration was 0.2 M. Also, a peak was found around 33 μm when 120 dm^3/h of pure CO_2 was supplied to the $CaCl_2$ solution with the highest initial concentration, i.e., 0.6 M.

The final particle size, both primary crystals and agglomerates, is a result of the course of a nucleation step, crystal growth and agglomeration and can be affected by the same variables that Kitamura mentioned as controlling the formation of polymorphs.[8,48] As a general rule, to produce fine particles, high supersaturation and intense mixing should be employed. A higher supersaturation leads to a smaller mean particle size since the nucleation rate is more sensitive to this parameter than the crystal growth rate.[33] Therefore, a decrease in the size of calcium carbonate particles with an increase of $CaCl_2$ concentrations was observed regardless of the type of reactor in which precipitation was

carried out. Mixing in both reactors was achieved by means of a gas flow. Higher gas flow results in more intensive mixing and a higher shear rate. Average shear rates in the bubble column were estimated using the method proposed by Sánchez Pérez et al.[49]:

$$\gamma = \left(\frac{1}{\mu}\frac{P}{V}\right)^{1/2} \tag{7}$$

where γ is an average share rate, μ is a liquid viscosity, and P/V is a power input per unit volume of liquid that is related to the superficial gas velocity, U_G, as follows:

$$\frac{P}{V} = \rho g U_G \tag{8}$$

where ρ is the density of fluid. Calculated values of an average shear rate varied from about 200–350 1/s when the gas flow was in the range of 60–180 dm³/h. Similar values were obtained for the gas-lift reactor when the superficial velocity in the riser U_{GR} was used for the calculations and the power input was corrected according to Chisty and Moo-Young[50]:

$$\frac{P}{V} = \rho g U_{GR} \frac{A_r}{A_r + A_d} \tag{9}$$

where A_r and A_d are a riser cross-section area and a downcomer cross-section area, respectively. The influence of mixing intensity on the mean particle size was not significant in the investigated range of gas flow rate. A slight reduction in the particle size was only observed for the highest gas flow rate. The formation of secondary agglomerates was observed mostly in the gas-lift reactor for both a low gas flow rate and a high $CaCl_2$ concentration. This type of reactor is characterized by a high ordered liquid circulation, the lower gas holdup and less intense mixing relative to a bubble column.[44] In addition, two main zones are generated in the gas-lift reactor during the gas flow: a riser and a downcomer, which differ in gas holdups. Values of this parameter are always higher in the riser; therefore, a mass transfer is more effective in this zone, and the variation of the rate of carbon dioxide transfer from gas to the liquid phase can affect the local inhomogeneity of supersaturation in the gas-lift reactor, which can contribute to crystal agglomeration.

CONCLUSION

Selection of the appropriate reactor to conduct precipitation in a gas–liquid system allows controlling the hydrodynamic condition during the reaction and generating a gas–liquid contact enabling a good mass transfer from a gas to liquid phase and enough liquid circulation to avoid settling of the produced vaterite particles. In this work, the precipitation process was carried out in the bubble column or in the gas-lift reactor with internal circulation, which is a modified construction of a bubble column, by placing a draft tube coaxially in relation to the outer column. The reaction time was slightly increased when the gas-lift reactor was used in the case of a low gas flow rate, high calcium chloride concentration and lower volume fraction of carbon dioxide in the supplying gas stream in the investigated range of parameters. The effect of mixing intensity on the mean size of synthesized vaterite particles was not significant in both investigated systems. Small deformation of spherical vaterite particles was observed more frequently when precipitation was carried out in a bubble column. Secondary agglomerates were formed in the gas-lift reactor for a low carbon dioxide flow rate or high calcium chloride concentration in the initial solution, probably as a result of the variation in carbon dioxide absorption in a riser and a downcomer, and hence inhomogeneous local supersaturation, which may promote agglomeration. Summarizing, calcium carbonate containing mainly vaterite was obtained in both tested reactors. However, the production of homogeneous spherical particles without the formation of agglomerates in a gas-lift reactor required careful selection of the calcium chloride concentration, the CO_2 content in the gas mixture and the mixing intensity.

CONFLICT OF INTEREST

The authors declare that they have no conflict of interest

ELECTRONIC SUPPLEMENTARY MATERIAL

The online version of this article (https://doi.org/10.1007/s11837-018-3307-0) contains supplementary material, which is available to authorized users.

REFERENCES

1. J. Chen and L. Xiang, *Powder Technol.* 189, 64 (2009).
2. D. Kralj, L. Brecevic, and J. Kontrec, *J. Cryst. Growth* 177, 248 (1997).
3. A.G. Christy, *Cryst. Growth Des.* 17, 3567 (2017).
4. D.B. Trushina, T.V. Bukreeva, and M.N. Antipina, *Cryst. Growth Des.* 16, 1311 (2016).
5. N. Qiu, H. Yin, B. Ji, N. Klauke, A. Glidle, Y. Zhang, H. Song, L. Cai, L. Ma, G. Wang, L. Chen, and W. Wang, *Mater. Sci. Eng., C* 32, 2634 (2012).
6. D.B. Trushina, T.V. Bukreeva, M.V. Kovalchuk, and M.N. Antipina, *Mater. Sci. Eng., C* 45, 644 (2014).
7. V. Lauth, M. Maas, and K. Rezwan, *Mater. Sci. Eng., C* 78, 305 (2017).
8. M. Kitamura, *CrystEngComm* 11, 949 (2009).
9. J. Prah, J. Maček, and G. Dražič, *J. Cryst. Growth* 324, 229 (2011).
10. Q. Li, Y. Ding, F. Li, B. Xie, and Y. Qian, *J. Cryst. Growth* 236, 357 (2002).
11. M.A. Popescu, R. Isopescu, C. Matei, G. Fagarasan, and V. Plesua, *Adv. Powder Technol.* 25, 500 (2014).
12. I. Udrea, C. Capat, E.A. Olaru, R. Isopescu, M. Mihai, C.D. Mateescu, and C. Bradu, *Ind. Eng. Chem. Res.* 51, 8185 (2012).
13. Z. Zhang, B. Yang, H. Tang, X. Chen, and B. Wang, *J. Mater. Sci.* 50, 5540 (2015).
14. K.S. Seo, C. Han, J.H. Wee, J.K. Park, and J.W. Ahn, *J. Cryst. Growth* 276, 680 (2005).
15. Y.S. Han, G. Hadiko, M. Fuji, and M. Takahashi, *J. Cryst. Growth* 289, 269 (2006).
16. P.-C. Chen, C.Y. Tai, and K.C. Lee, *Chem. Eng. Sci.* 52, 22 (1997).
17. A.G. Jones, *Crystallization Process Systems* (Oxford: Butterworth-Heinemann, 2002).
18. K. Wang, Y.J. Wang, G.G. Chen, G.S. Luo, and J.D. Wang, *Ind. Eng. Chem. Res.* 46, 6092 (2007).
19. D. Konopacka-Łyskawa, Z. Cisiak, and B. Kawalec-Pietrenko, *Powder Technol.* 190, 319 (2009).
20. S.H. Kang, S.G. Lee, W.M. Jung, M.C. Kim, W.S. Kim, C.K. Choi, and R.S. Feigelson, *J. Cryst. Growth* 254, 196 (2003).
21. M. Altiner and M. Yildirim, *Adv. Powder Technol.* 28, 553 (2017).
22. F.P. Carr and D.K. Frederick, *Kirk-Othmer Encycl. Chem. Technol.* 4, 551 (2012).
23. D. Konopacka-Łyskawa, B. Kościelska, J. Karczewski, and A. Gołąbiewska, *Mater. Chem. Phys.* 193, 13 (2017).
24. M. Vučak, J. Perić, and R. Krstulović, *Powder Technol.* 91, 69 (1997).
25. Q. Liu, H.S. Wang, and Q. Zeng, *J. Cryst. Growth* 449, 43 (2016).
26. W. Hou and Q. Feng, *Mater. Sci. Eng., C* 26, 644 (2006).
27. H. Guo, Z. Qin, P. Qian, P. Yu, S. Cui, and W. Wang, *Adv. Powder Technol.* 22, 777 (2011).
28. M. Faatz, F. Gröhn, and G. Wegner, *Mater. Sci. Eng., C* 25, 153 (2005).
29. M. Ukrainczyk, J. Kontrec, V. Babić-Ivančić, L. Brečević, and D. Kralj, *Powder Technol.* 171, 192 (2007).
30. W. Bao, H. Li, and Y. Zhang, *Cryst. Res. Technol.* 44, 395 (2009).
31. Y. Wen, L. Xiang, and Y. Jin, *Mater. Lett.* 57, 2565 (2003).
32. D. Gomez-Diaz, J.M. Navaza, and B. Sanjurjo, *Chem. Eng. J.* 116, 203 (2006).
33. S. Wachi and A.G. Jones, *Chem. Eng. Sci.* 46, 3289 (1991).
34. S. Riglopoulus and A.G. Jones, *Chem. Eng. Sci.* 56, 6177 (2001).
35. K. Tamura and H. Tsuge, *Chem. Eng. Sci.* 61, 5818 (2006).
36. J.R. Burns and R.J.J. Jachuck, *AIChE J.* 51, 1497 (2005).
37. W.M. Jung, S.H. Kang, K.S. Kim, W.S. Kim, and C.K. Choi, *J. Cryst. Growth* 312, 3331 (2010).
38. K. Kędra-Królik and P. Gierycz, *J. Therm. Anal. Calorim.* 83, 579 (2006).
39. S. Varma, P.C. Chen, and G. Unnikrishnan, *Mater. Chem. Phys.* 126, 232 (2011).
40. F. Kang, D. Wang, Y. Pu, X.F. Zeng, J.X. Wang, and J.F. Chen, *Powder Technol.* 325, 405 (2018).
41. J.C. Merchuk and M. Gluz, *Encyclopedia of Bioprocess Technology*, eds. M.C. Flickinger and S.W. Drew (New York: Wiley, 1999), pp. 320–353.
42. F. Mani, M. Peruzzini, and P. Stoppioni, *Green Chem.* 8, 995 (2006).
43. O. Sohnel and J.W. Mullin, *J. Cryst. Growth* 60, 239 (1982).
44. J.M. van Baten and R. Krishna, *Chem. Eng. Technol.* 26, 1074 (2003).
45. A. Sanchez Miron, M.-C. Ceron Garcia, F. Garcia Camacho, E. Molina Grima, and Y. Chisti, *Chem. Eng. Res. Des.* 82, 1367 (2004).
46. C.G. Kontoyannis and N.V. Vagenas, *Analyst* 125, 251 (2000).
47. J.D. Rodriguez-Blanco, S. Shaw, and L.G. Benning, *Nanoscale* 3, 265 (2011).
48. D.J. Wedlock, *Controlled Particle, Droplet and Bubble Formation* (Oxford: Butherworth-Heinemann, 1994).
49. J.A. Sánchez Pérez, E.M. Rodríguez Porcel, J.L. Casas López, J.M. Fernández Sevilla, and Y. Chisti, *Chem. Eng. J.* 124, 1 (2006).
50. Y. Chisti and M. Moo-Young, *Biotechnol. Bioeng.* 34, 1391 (1989).